Electronic Supplementary Material (ESI) for Journal of Materials Chemistry A.
This journal is © The Royal Society of Chemistry 2019

Supporting Information for

Boosting Performance of Fe-N-C Catalyst for Oxygen Reduction Reaction by Introducing Single-Walled Carbon Nanohorns as Branches on Carbon Fibers

Jianshuo Zhang[a,c], Yang Liu[a,c], Zhoubin Yu[b], Meihua Huang[a], Chuxin Wu[a], Chuanhong Jin[b] and Lunhui Guan[a]*

a. CAS Key Laboratory of Design and Assembly of Functional Nanostructures, and Fujian Provincial Key Laboratory of Nanomaterials, Fujian Institute of Research on the Structure of Matter, Chinese Academy of Sciences, Fuzhou, Fujian 350002, P.R. China

b. State Key Laboratory of Silicon Materials, School of Materials Science and Engineering, Zhejiang University, Hangzhou, Zhejiang 310027, China

c. University of Chinese Academy of Sciences (UCAS), Beijing 100049, P.R. China

† Corresponding Author: guanlh@fjirsm.ac.cn

Experimental

Materials and methods

Polyacrylonitrile (PAN) was purchased from J&K Scientific Ltd. Zinc chloride ($ZnCl_2$), *N*, *N*-Dimethylformamide (DMF) and hydrochloric acid aqueous solution (HCl) were purchased from Sinopharm Chemical Reagent Co. Ltd. Nafion ionomer (5 wt%) was purchased from Aldrich. Potassium hydroxide (KOH, 95%) and Hemin($C_{34}H_{32}ClFeN_4O_4$) were purchased from MERYER Co.Ltd. QAPS Membrane and the corresponding ionomer solution were purchased from Hephasenergy.com. SWCNHs were produced in our lab by arc-discharge method. Pt/C (20 wt% HiSPEC™ 3000) was purchased from Johnson Matthey Company.

Synthetic procedures

Preparation of FeNCF. 100 mg of hemin and 0.4 g of PAN was added into the solution under 80 ℃ with magnetic stirring. After stirring overnight, the precursor mixture was loaded into a plastic syringe (10 mL). After the same electrospinning step mentioned above, the as-electrospun PAN/Hemin/SWCNH precursor networks were placed in a vacuum oven for 6 h at 90 °C in order to remove the solvent residuals, and then calcinated in the air at 250 °C for 1h with a ramping rate of 1 °C /min. After the same pyrolysis and etching steps, the final FeNCF was obtained.

Preparation of FeNCF w $ZnCl_2$. 50 mg of $ZnCl_2$ and 100 mg of hemin were distributed into 5g DMF solvent and then 0.4 g of PAN was added into the solution under 80 ℃ with magnetic stirring. After stirring overnight, the precursor mixture was loaded into a plastic syringe (10 mL). After a same electrospinning step mentioned above. The as-electrospun precursor networks were placed

in a vacuum oven for 6 h at 90 °C in order to remove the solvent residuals, and then they were calcinated in the air at 250 °C for 1h with a ramping rate of 1 °C min^{-1}. After the same pyrolysis and etching steps, the final FeNCF w $ZnCl_2$ sample was obtained.

Preparation of FeNCF w SWCNH. 100 mg of SWCNHs and 100 mg of hemin were distributed into 5g DMF solvent and then 0.4 g of PAN was added into the solution under 80 ℃ with magnetic stirring. After stirring overnight, the precursor mixture was loaded into a plastic syringe (10 mL). After a same electrospinning step mentioned above. The as-electrospun PAN/Hemin/SWCNH precursor networks were placed in a vacuum oven for 6 h at 90 °C in order to remove the solvent residuals, and then they were calcinated in the air at 250 °C for 1h with a ramping rate of 1 °C /min. After the same pyrolysis and etching steps, the final FeNCF w SWCNH sample was obtained.

Preparation of FeNCF w (X%$ZnCl_2$+SWCNH). The iron-nitrogen co-doped carbon fibers (FeNCF) with different porosity were synthesized by electrospinning technology. In a typical procedure, different contents of $ZnCl_2$ (4%, 8%, 14%, 25%), 100 mg of hemin and 100 mg of SWCNHs were distributed into 5g DMF solvent and then 0.4 g of PAN was added into the solution under 80 °C with magnetic stirring. After stirring overnight, the precursor mixture was loaded into a plastic syringe (10 mL). A voltage of 24 kV was applied for electrospinning with the controlled flow rate at 0.1 mL min^{-1}. The aluminum foil was used as another pole piece for collecting the preliminary product. The distance between the orifice and the aluminum foil electrode was 20 cm. The as-electrospun PAN/Hemin/SWCNH precursor networks were placed in a vacuum oven for 6 h at 90 °C in order to remove the solvent residuals, and then they were calcinated in the air at 250 °C for 1h with a ramping rate of 1 K min^{-1}. Then, the pre-treatment samples were first pyrolysis at 700 °C in nitrogen

atmosphere for 3 h with a ramping rate of 2 °C min^{-1}. After acid etching at 80 ℃ for 8 h. The samples were pyrolysis at 950 °C for another 3 h in nitrogen atmosphere with a ramping rate of 5 °C min^{-1}. The final samples were denoted as **FeNCF w (X%$ZnCl_2$+SWCNH)** (X value represents the mass ratio of $ZnCl_2$ in all solid substance).

Physical characterization

Scanning electron microscopy (SEM) characterization were performed with a field emission scanning electron microscope (FESEM SU8010). Transmission electron microscopy (TEM), high resolution transmission electron microscopy (HRTEM), high-annular dark-field scanning transmission electron microscopy (STEM) and element mapping analysis were conducted on FEI, JEM-2010 electron microscope operating at 200 kV. X-ray diffraction (XRD) measurements were performed with a Miniflex600 diffractometer using a Cu Kα (λ = 1.5405 Å) radiation source. Raman spectra were collected on a LabRAM HR spectrometer with 633 nm wavelength incident laser light. X-ray photoelectron spectroscopy (XPS) analysis was performed with an ESCALAB 250Xi X-ray photoelectron spectrometer (Thermo, America). The pore structures of the samples were analyzed by using an Autosorb-iQ2 (Quantachrome Instruments) physical absorber.

Electrochemical measurements

Rotating Disk Electrode tests. All electrocatalytic measurements were performed in a three-electrode cell using a rotating disk electrode (RDE, PINE Research Instrumentation) of 5.0 mm in diameter with an electrochemical workstation (CHI 760D, Shanghai Chenhua, China) in 0.1M KOH electrolyte. A platinum wire and Ag/AgCl (saturated KCl) electrode were used as the counter and reference electrodes, respectively. All potentials in this study are referenced to reversible hydrogen electrode (RHE), E(RHE) = E(Ag/AgCl) + 0.059pH + 0.197. The catalyst ink is prepared by

dispersing the catalyst (5 mg) in solution (1 mL) containing isopropanol (0.95 mL) and 5 wt% Nafion solution (50 uL), followed by ultrasonication for 30 min. Then, a certain volume of catalyst ink was pipetted onto the GC surface to give a 0.35 mg cm^{-2} loading for all samples. The loading of commercial Pt/C (20 wt%, Johnson Matthey) was 20 ug_{Pt} cm^{-2}. Prior to testing, the electrolyte was saturated with oxygen by bubbling O_2 and a flow of O_2 was maintained over the electrolyte during the measurements. Cyclic voltammetry (CV) and linear sweep voltammetry (LSV) curves of the catalyst under N_2-saturated alkaline electrolyte were also measured. The scan rate of LSV was 10 mV s^{-1} and the rotating speed was varied from 500 to 2500 rpm. For the ORR on a RDE, the electron transfer numbers can be calculated with Koutecky-Levich equations:

$$1/J = 1/J_L + 1/J_K = 1/(B\omega^{1/2}) + 1/J_K$$

where J is the measured current density; and JK are the kinetic and JL diffusion-limiting current densities, respectively; ω is the angular velocity of the disk (ω = 2πN, N is the linear rotation speed).

$$B = 0.2nFC_0(D_0)^{2/3}v^{-1/6}$$

$$J_K = nFKC_0$$

where n represents the transferred electron number; F is the Faraday constant (F = 96485 C mol^{-1}); C_0 is the bulk concentration of O_2 (1.2×10^{-6} mol cm^{-3}); D_0 is the diffusion coefficient of O_2 in 0.1 M KOH electrolyte (1.9×10^{-5} cm^2 s^{-1}); v is the kinematics viscosity for electrolyte (0.01 cm^2 s^{-1}), and k is the electron-transferred rate constant.

Supporting Figures

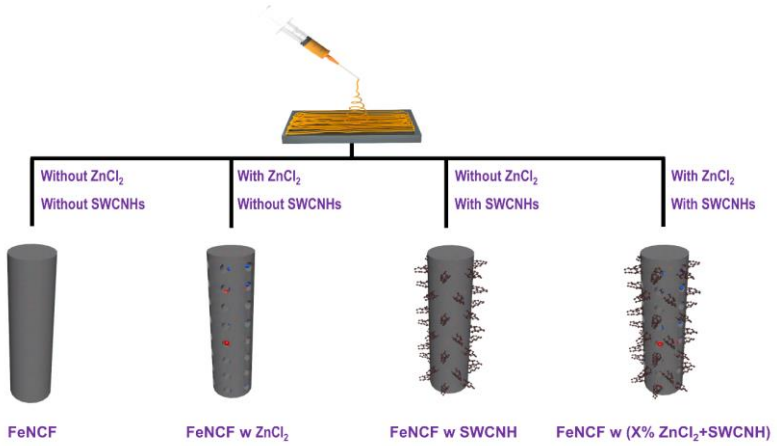

Figure S1 A schematic diagram that described the pore-forming effect of zinc chloride and SWCNHs. In this study, we introduced single-walled carbon nanohorns (SWCNHs) into the electrospinning process to increase the specific surface area (SSA) and pore volume of the carbon fibers. SWCNHs can not only provide electrical conductivity networks, but also help to create a relatively narrow distribution of mesopores (pore width ≈2-5 nm) during the pore constructing process with zinc chloride

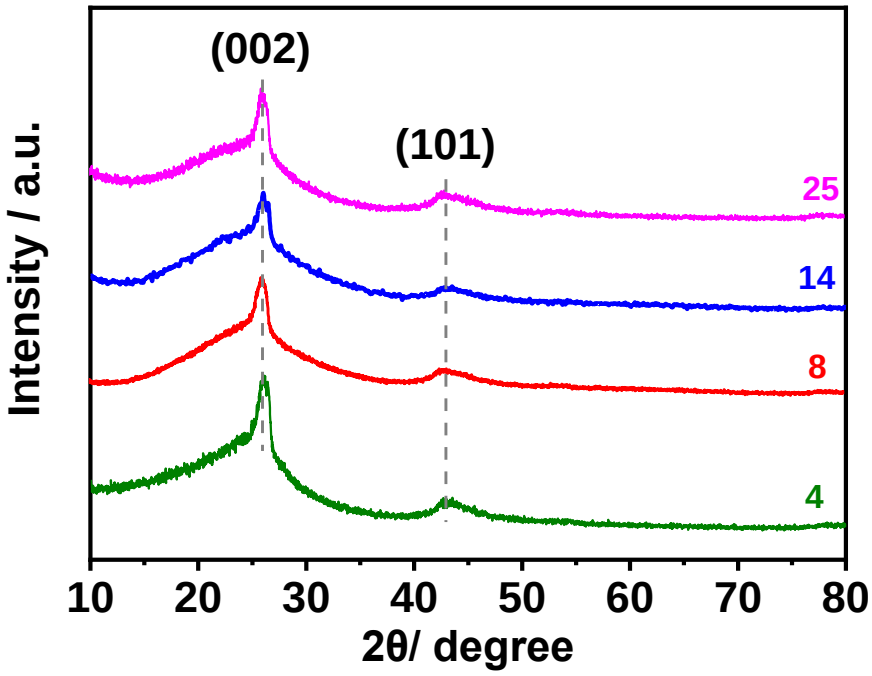

Figure S2 PXRD patterns of FeNCF w (X%$ZnCl_2$+SWCNH) samples (**The colorful number is the value of X**). The compared samples fabricated with different $ZnCl_2$ mass contents exhibit similar XRD patterns. For the typical pattern, the peaks centered at 26.2° and 42.7° were assigned to the (002) and (101) planes of graphitic carbon. No obvious diffraction peaks about iron and zinc were observed, indicating that metallic state iron and zinc are excluded.

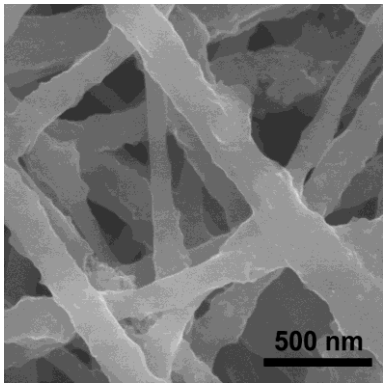

Figure S3 The SEM image of FeNCF w (8%$ZnCl_2$+SWCNH) catalyst.

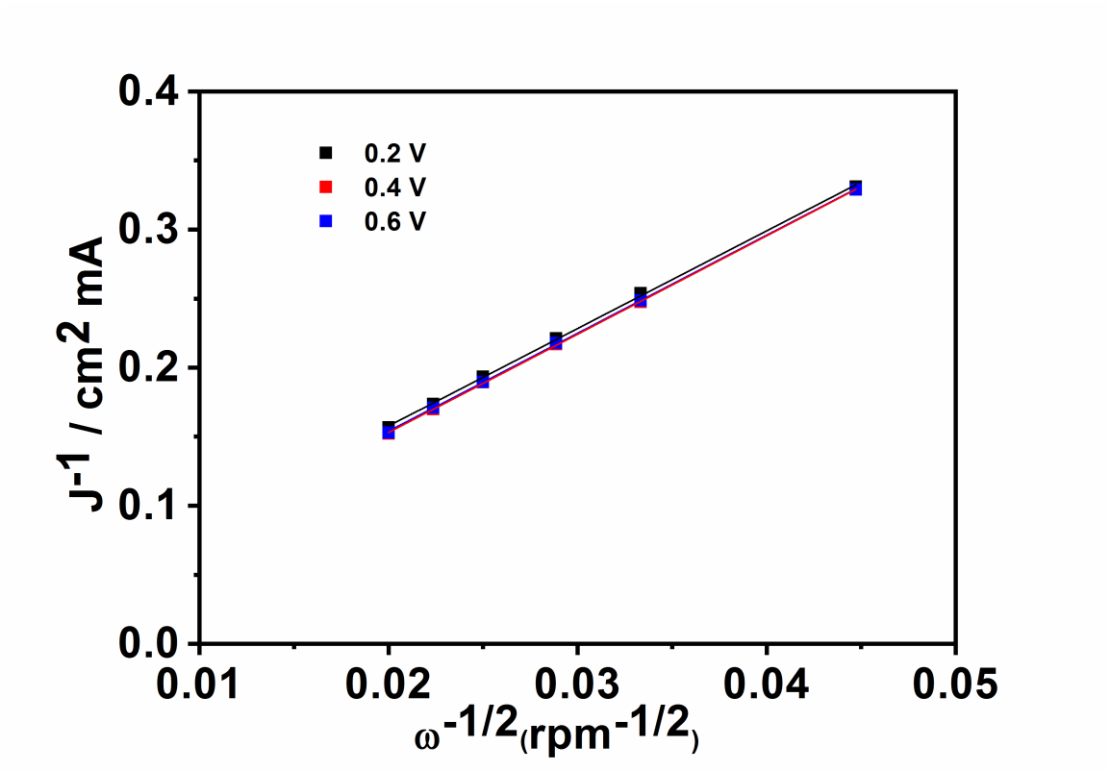

Figure S4 K-L plots of FeNCF w (8%$ZnCl_2$+SWCNH) sample.

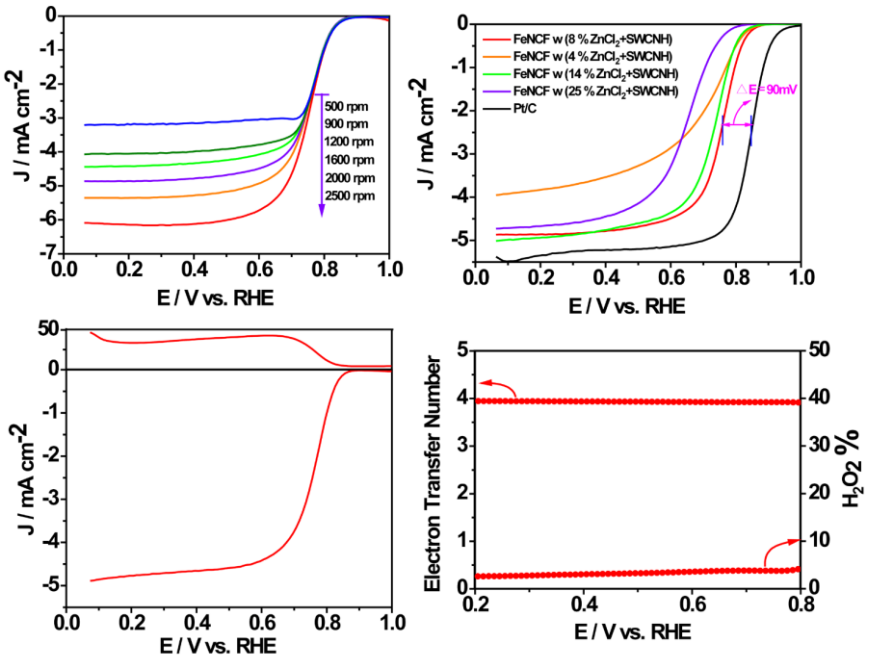

Figure S5 (a) ORR performance of FeNCF w (8%$ZnCl_2$+SWCNH) sample recorded in O_2-saturated 0.1 M $HClO_4$ solution at room temperature.

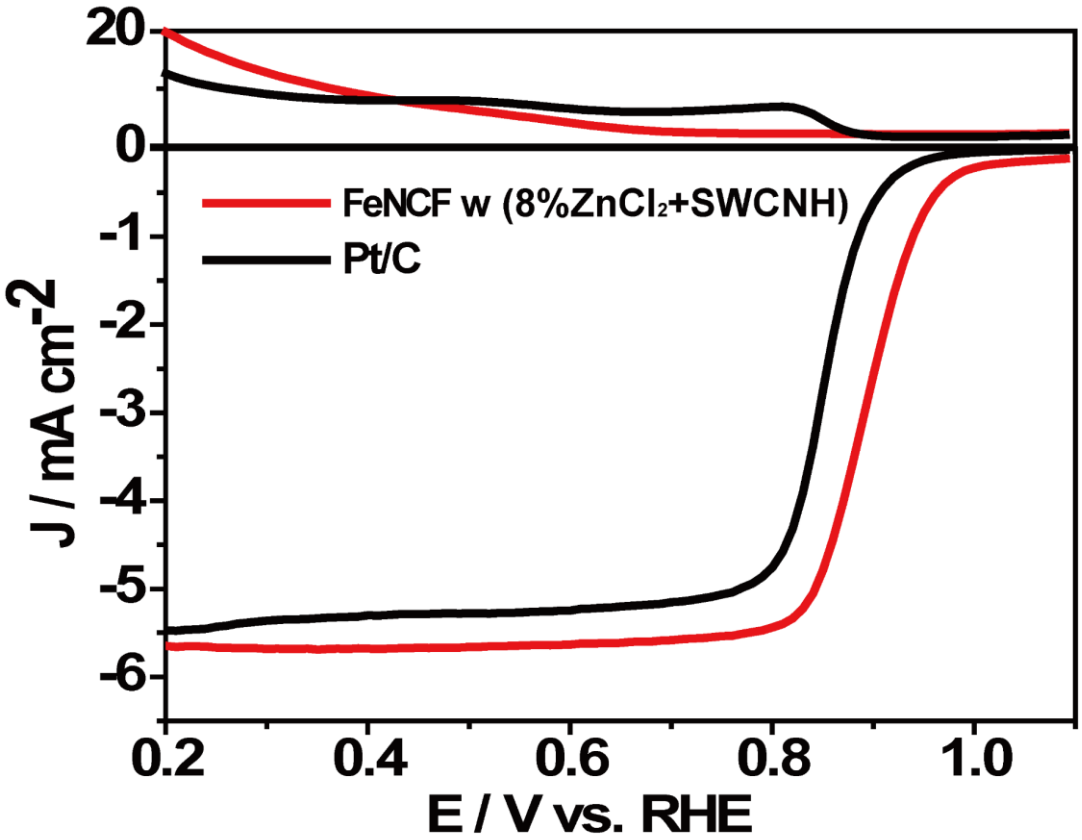

Figure S6 LSV plots of FeNCF w (8%$ZnCl_2$+SWCNH) and Pt/C recorded on a RRDE.

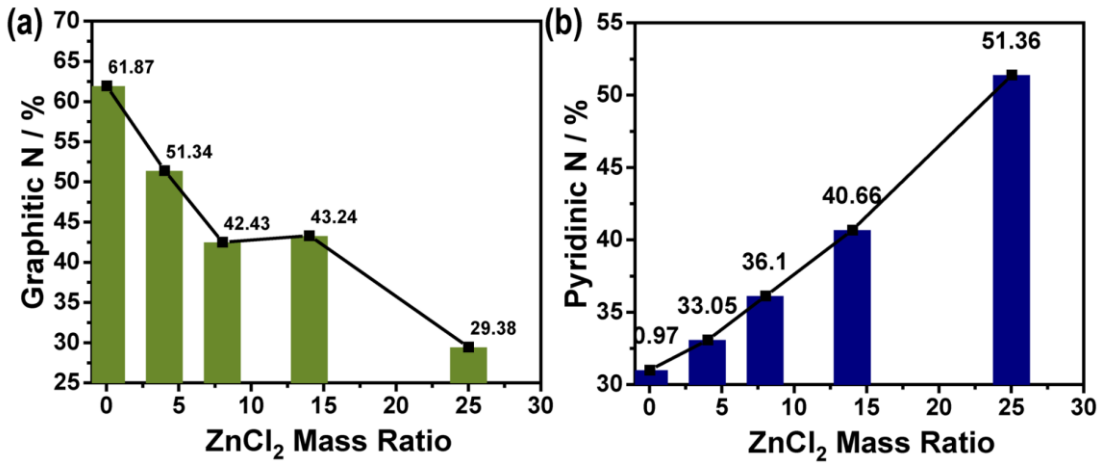

Figure S7 Line charts of relationship between the content of different types of nitrogen and $ZnCl_2$ dosage (graphitic N for Figure a and pyridinic N for Figure b).

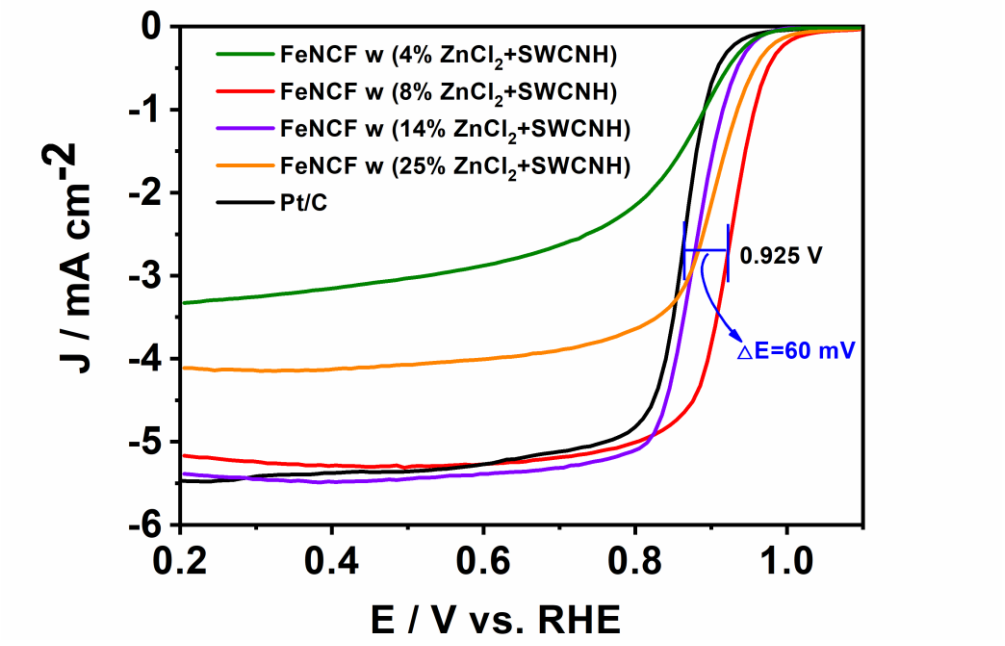

Figure S8 LSV plots of FeNCF w (X%$ZnCl_2$+SWCNH) and Pt/C catalysts recorded on a RDE at room temperature with a rotation rate of 1600 rpm.

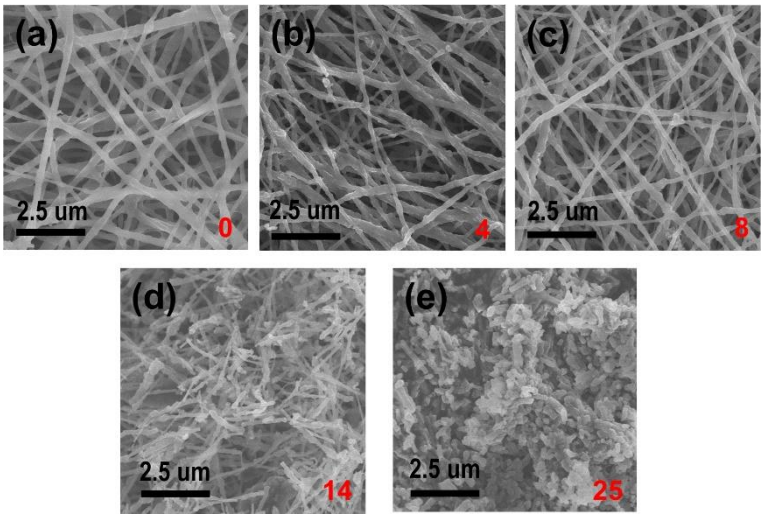

Figure S9 SEM images of FeNCF w (X%$ZnCl_2$+SWCNH) samples. The red number in the figure is the corresponding X values of these samples. FeNCF w (0%$ZnCl_2$+SWCNH) sample is same as FeNCF w SWCNH sample.

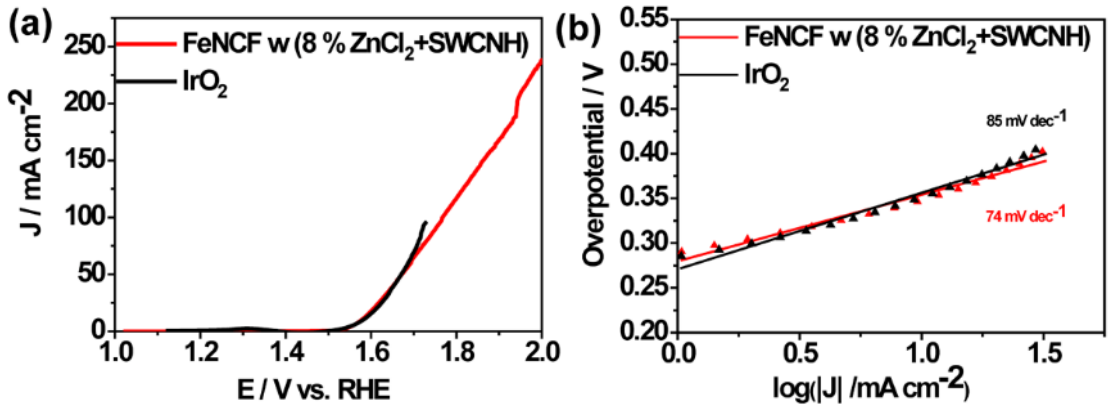

Figure S10 OER performance of FeNCF w (8%$ZnCl_2$+SWCNH) and IrO_2 catalysts.

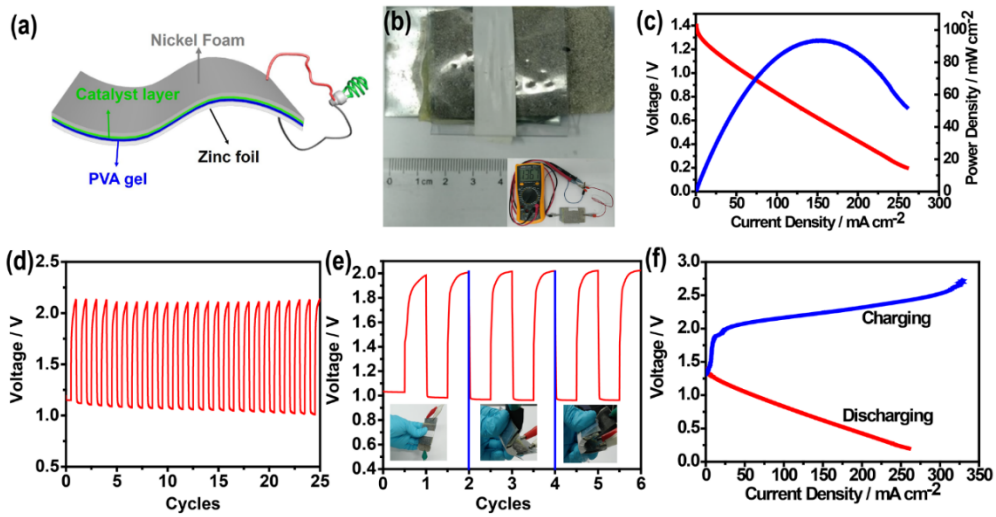

Figure S11 The performance of a flexible Zn-air battery.

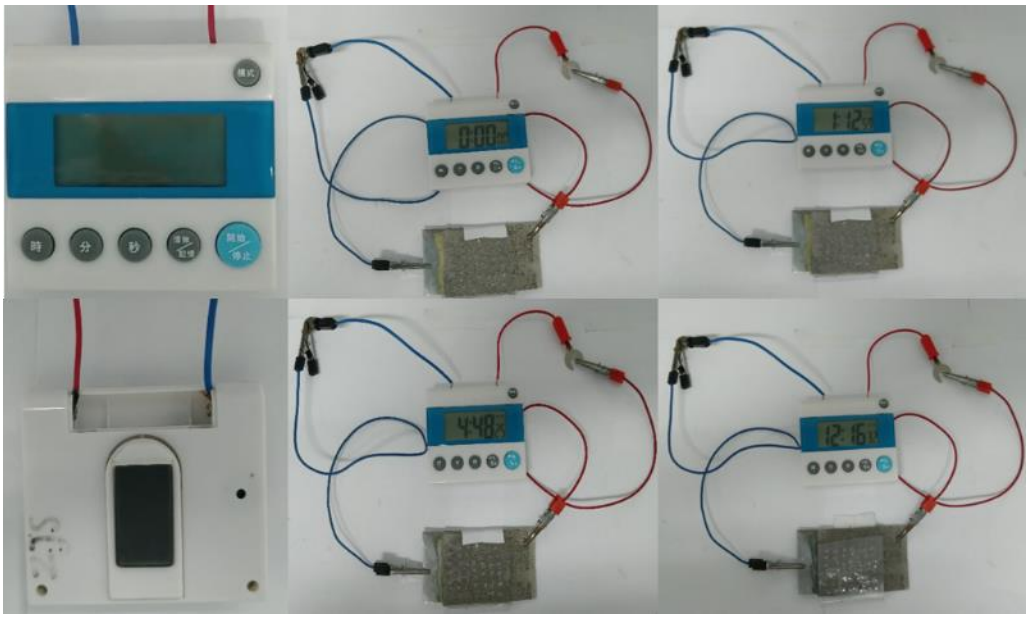

Figure S12 Photographs of a timer recorded at different times.

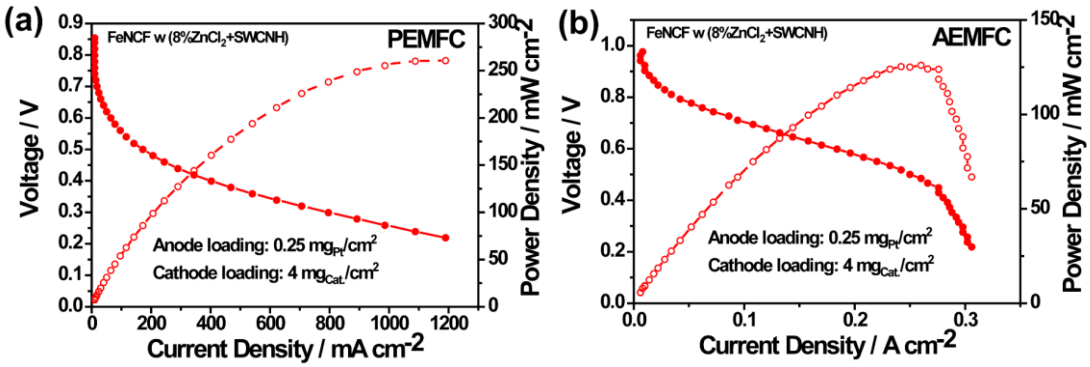

Figure S13 The H_2-O_2 fuel cell performance of FeNCF w (8%$ZnCl_2$+SWCNH) catalyst (Humidity:100%, Backpressure: 1 bar, H_2 flow rate: 200 sccm, O_2 flow rate: 400 sccm).

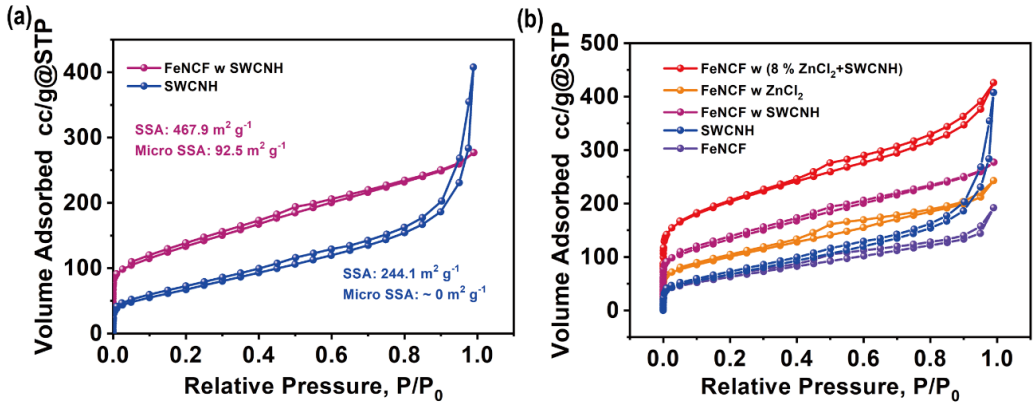

Figure S14 N_2-adsorption/desorption isotherms of FeNCF w (8%$ZnCl_2$+SWCNH), FeNCF w $ZnCl_2$, FeNCF w SWCNH, FeNCF and SWCNH samples**.** After adding SWCNH only to FeNCF, FeNCF w SWCNH exhibits higher adsorbed volume than itself, indicated that SWCNH has the function of making mesopores and macropores. However, the role of SWCNH has not been fully utilized in the absence of $ZnCl_2$, and vice versa. Only with the joint addition of $ZnCl_2$ and SWCNH can the material perform the most effective results (FeNCF w (8% $ZnCl_2$ + SWCNH)). Previous work have proved that the catalytic activity of the edge active sites (Edge hosted Fe-N_4) is higher than that of the internal active sites (***Science 357, 2017, 479-484; J. Am. Chem. Soc. 140, 2018, 11594-11598***). The combination of SWCNH and $ZnCl_2$ makes the FeNCF w (8% $ZnCl_2$ + SWCNH) has a very rich pore structure. Hence, FeNCF w (8% $ZnCl_2$ + SWCNH) has more edge defects in the case of ensuring mass transfer. Edge defects are more likely to form edge active sites. Hence, we think that having more edge active sites is the origin of high performance for the FeNCF w (8% $ZnCl_2$ + SWCNH).

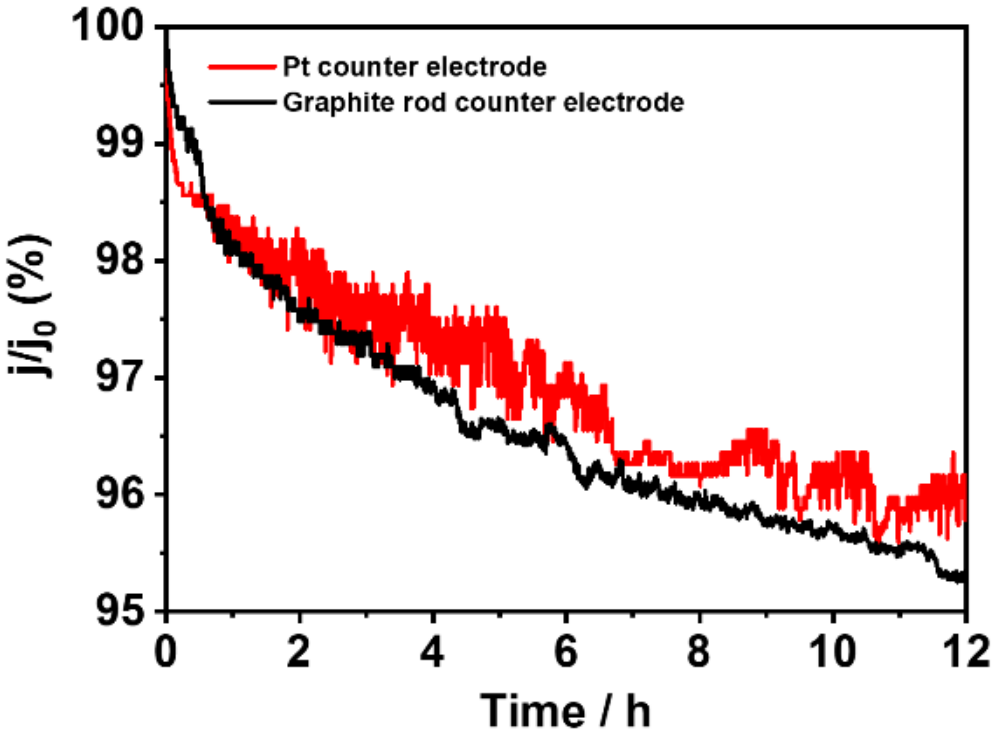

Figure S15 Stability plots of FeNCF w (8%$ZnCl_2$+SWCNH) using different counter electrodes. This is a picture with the y-axis zoomed in.

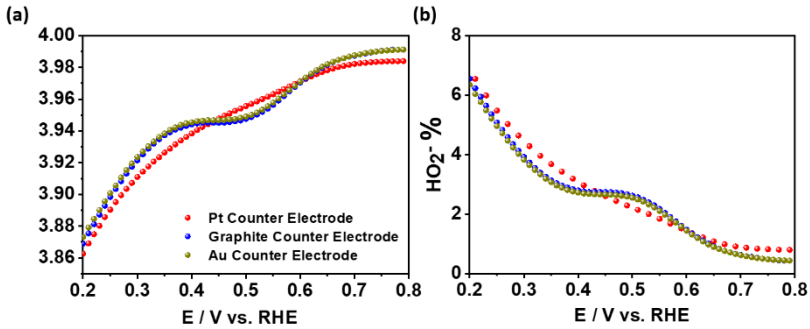

Figure S16 Electron transfer (a) and HO_2^- selectivity (b) plots of FeNCF w (8%$ZnCl_2$+SWCNH) using different counter electrodes.

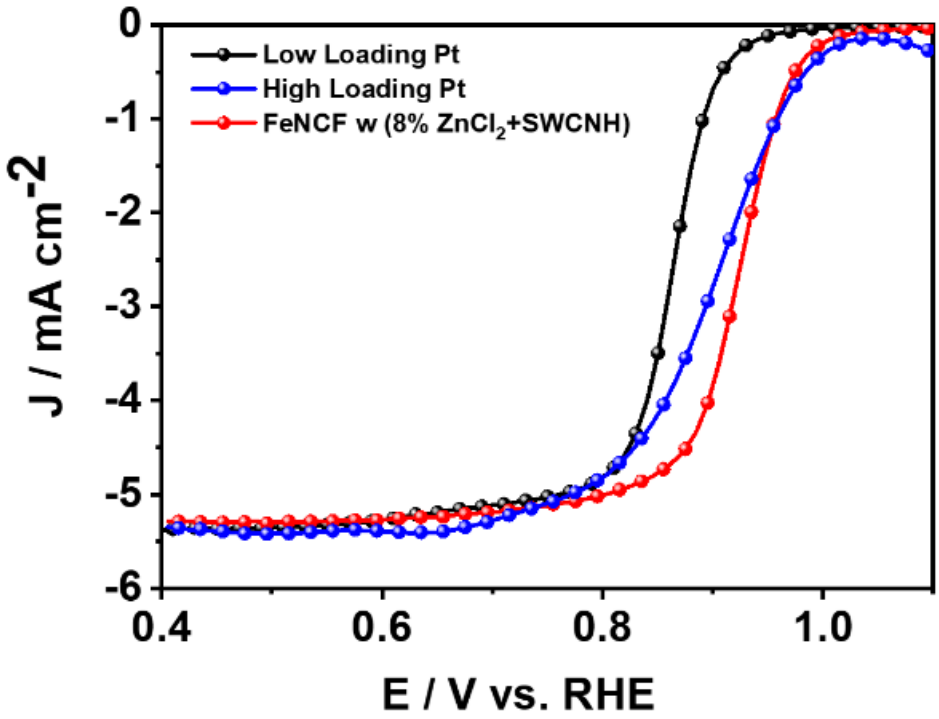

Figure S17 A comparison of LSV plots for low loading, high loading and the FeNCF w (8%$ZnCl_2$+SWCNH) sample. The half wave potential of FeNCF w (8%$ZnCl_2$+SWCNH) is 20 mV higher than that of high loading Pt/C (The loading of Pt/C is same with the FeNCF w (8%$ZnCl_2$+SWCNH) sample). However, the reason why we use the curve of low Pt loading as a comparison is to be consistent with the mainstream literature. There are many related studies that use lower loading Pt as a comparison (***Science 362, 1276-1281 (2018); Science 354, 1414-1419 (2016); J. Am. Chem. Soc. 2016 138 45 15046-15056; J. Mater. Chem. A, 2019, 7, 11223***). We believe that the reason for this choice is that a very small amount of platinum can achieve the well-recognized results, there is no need to do experiments with high loading.

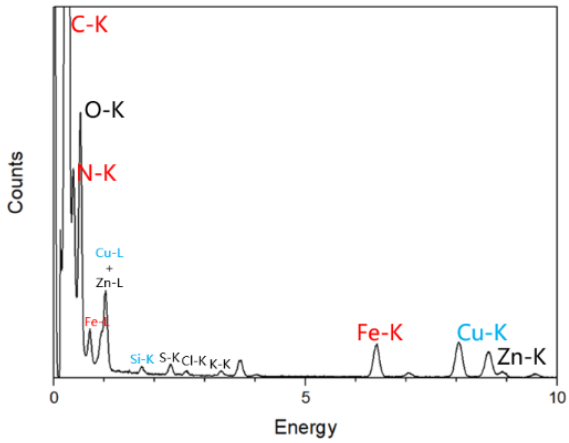

Figure S18 STEM-EDS spectrum of FeNCF w (8%$ZnCl_2$+SWCNH) sample. The Cu element comes from grid, the Si element comes from the probe of instrument. There are trace Zn in FeNCF w (8%$ZnCl_2$+SWCNH) sample. In recent years, related studies have shown that Zn has a catalytic effect on ORR (***Angew. Chem. Int. Ed. 2019, 58, 7035-7039; Adv. Funct. Mater. 2017, 27, 1700802; Chem.Commun.,2017,53, 11453-11456***). Song et al. reported the Zn single atom catalyst for the oxygen reduction reaction process in 2017. In the study, the free energy diagram for the oxygen reduction reaction on Zn-N_4 site and the ORR overpotential was computed to illuminate the reaction pathways and the catalytic activity. The ORR overpotential on Zn-N_4 site was computed to be about 1.70 V, close to the upper limit of 1.68 V for commercial Pt/C (0.69-1.68 V), further confirming the observed high ORR performance reported in the literature. Li et al. reported a kind of Zn-N_2 site observed in carbon materials. The corresponding theoretical calculations reveal that the structural activation of oxygen species on Zn-N_2 active sites is favored by the selective oxygen reduction (***Nature communications, 2019, 10, 2623***.). However, the above explanation may not appropriate, when considering whether **trace** amounts of Zn have an effect on the ORR, because iron and nitrogen doping is crucial. Lu et al. reported an isolated Zn-Co atomic pair for highly active and

durable oxygen reduction (***Angew. Chem. Int. Ed. 2019, 58, 2622-2626***). Such architecture offers enhanced binding ability of oxygen molecule, significantly elongates the O-O bond length (from 1.23 Å to 1.42 Å), and thus facilitates the cleavage of O-O bond, showing a theoretical overpotential of 0.335 V during ORR process. Hence, we think Zn and Fe atoms may form similar isolated Zn-Fe atomic pair to enhance the ORR activity in our study. Such Zn-Fe atomic pair architecture offers enhanced binding ability of oxygen molecule, elongates the O-O bond length to a certain degree, and thus facilitates the breakage of O-O bond.

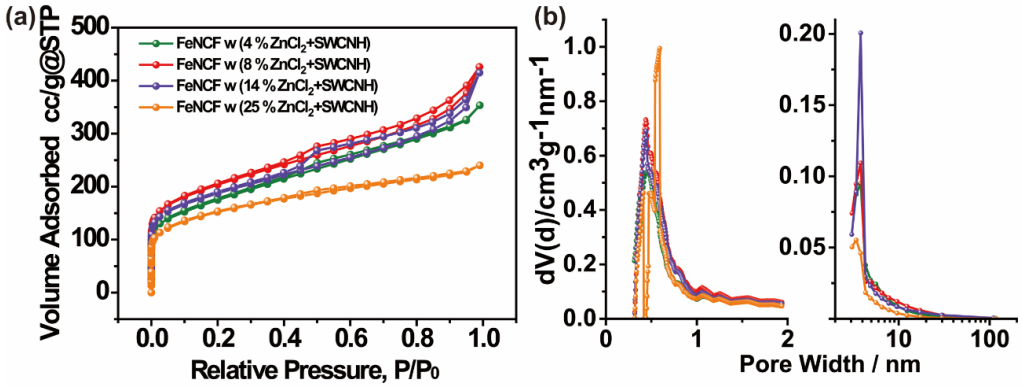

Figure S19 The isotherms of FeNCF w (X%$ZnCl_2$+SWCNH) after overlaying.

Discussion S1

As shown in Figure S14a, the SSA and Micro SSA of SWCNH is 244.1 m^2 g^{-1} and 0 m^2 g^{-1}, respectively; the SSA and Micro SSA of FeNCF w SWCNH is 467.9 m^2 g^{-1} and 92.5 m^2 g^{-1}, respectively. SWCNH is richer in mesopores and macropores as it has bigger adsorbed volume at higher relative pressure. After adding SWCNH only to FeNCF, FeNCF w SWCNH exhibits higher adsorbed volume than itself, indicated that SWCNH has the function of making mesopores and macropores. However, the role of SWCNH has not been fully utilized in the absence of $ZnCl_2$, and vice versa. Only with the joint addition of zinc chloride and SWCNH can the material perform the most effective results (the isotherm of FeNCF w (8% $ZnCl_2$ + SWCNH) as shown in Figure S14b).

Discussion S2 A discussion about using the Pt as a counter electrode.

There is a debate going on about using the Pt as a counter electrode. For example, the Pt counter electrode is at an oxidizing potential in HER tests, where Pt can dissolve in both acid and alkaline during Pt oxidation and PtO_x reduction. The dissolved Pt in electrolyte is electrodeposited onto the working electrode and alters the electrochemical performance, especially for non-precious metal catalyst, where even a small amount of Pt deposition on the working electrode can result in erroneous activity reports (***J. Mater. Chem. A, 2015, 3, 13080; Adv. Mater. 2019, 31, 1806296***).

The seemingly high activity, which gets enhanced during long-term stability tests, could be induced by artefacts from the counter electrode. To avoid the concerns on Pt counter electrode, a glassy carbon or graphite rod is recommended by some researchers (***Adv. Mater. 2019, 31, 1806296***). In our work, ORR is also a reduction reaction. Hence, Pt counter electrode may affect the activity after long-term stability test. Herein, we provide a new stability data using **graphite rod** as a counter electrode (**Figure S15**). After 12 h stability test, the plot using graphite rod as counter electrode is attenuated by **only 0.5%** more than the line using Pt as counter electrode. This result shows that

using Pt as a counter electrode **does not cause a drastic change in properties** of FeNCF w (8%$ZnCl_2$+SWCNH) sample. It also proves the reliability of the data in the text.

Furthermore, we also provide electron transfer and 2 electron-product selectivity evidence of FeNCF w (8%$ZnCl_2$+SWCNH) using graphite rod or Au wire as a counter electrode, respectively (**Figure S16**). The results show that replacing different counter electrodes has no significant effect on these two data. This result support the high electron transfer number mentioned in the manuscript.

Table S1

Samples	Electrolyte	$E_{1/2}$(V)	Reference
FeNCF w (8%$ZnCl_2$+SWCNH)	0.1 M KOH	0.925	This Work
Fe–N–C HNSs	0.1 M KOH	0.87	Adv. Mater. 2018, 1806312
Co,N-PCL[4]	0.1 M KOH	0.846	Applied Catalysis B: Environmental 246 (2019) 322–329
Fe-N-S CNN	0.1 M KOH	0.91	Applied Catalysis B: Environmental 250 (2019) 143–149
Fe-NPC	0.1 M KOH	0.89	Applied Catalysis B: Environmental 249 (2019) 306–315
Fe-NMP	0.1 M KOH	0.84	Journal of Power Sources 375 (2018) 214-221
Cu-Fe-N-C	0.1 M KOH	0.864	Applied Catalysis B: Environmental 242 (2019) 209–217
Fe-ISA/SNC	0.1 M KOH	0.896	Adv. Mater. 2018, 30, 1800588
Fe-N-C	0.1 M KOH	0.89	Journal of Power Sources 375 (2018) 244-254
Fe SAs-N/C-20	0.1 M KOH	0.915	J. Am. Chem. Soc. 2018 140 (37), 11594-11598
FeNC-900	0.1 M KOH	0.851	Chem. Commun., 2018, 54, 1307-1310
Fe–N–C/rGO	0.1 M KOH	0.81 V	ACS Appl. Mater. Interfaces 2018, 103, 2423-2429
Fe-SAs/NPS-HC	0.1 M KOH	0.912	Nat. commun. 2018, 9(1), 5422.
Co-Fe/NC-700	0.1 M KOH	0.854	Small 2019, 1805324